Available online at website: https://journal.bcrec.id/index.php/bcrec

Bulletin of Chemical Reaction Engineering & Catalysis, 21 (1) 2026, 22-37

Original Research Article

Synthesis and Carbonization of Core-Shell ZIF-67@ZIF-90 for Ciprofloxacin and Azithromycin Removal

Fatimah Al-Ghazzawi[1]*, Mohammed Mahdi Al-Mossawi[2], Amjad Al-Shawi[3], Kadhim Al-Attafi[4]

[1]Al-Nasiriyah Technical Institute, Southern Technical University, Thi-Qar 64001, Iraq.
[2]Marine Geology Department, Marine Science Center, University of Basrah, Basrah, Iraq.
[3]Department of Physics, College of Education for Pure Science, University of Basrah, Basrah, Iraq.
[4]Department of Physics, College of Science, University of Kerbala, Karbala, Iraq.

Received: 26th September 2025; Revised: 1st November 2025; Accepted: 2nd November 2025
Available online: 12th November 2025; Published regularly: April 2026

Abstract

The elimination of antibiotics such as Azithromycin (AZM) and Ciprofloxacin (CIP) from the contaminated water is crucial to safeguard both human health and environmental quality. This study investigates the synthesis of CoNC@NC core-shell composite by carbonizing ZIF-67@ZIF-90 composite, and the implementation of them in removing antibiotics from aqueous solutions. The composites were characterized using XRD, SEM, FTIR, Raman, TGA, and N_2 adsorption-desorption. In the batch adsorption tests, the carbonized composite showed enhanced adsorption capacities compared to the original composite, with maximum adsorption capacities for AZM and CIP being 256.49 mg/g and 514.26 mg/g, respectively. The adsorption process was found to fit the pseudo-first-order kinetics and Langmuir isotherm models. The solution pH showed a significant impact on the adsorption capacity, with maximum capacities recorded at pH of 7 and 6 for the AZM and CIP solutions, respectively. In addition, it was demonstrated that after five regeneration cycles, the carbonized composite maintained the adsorption capacity at over 90% of the first cycle value, suggesting good reusability. These results revealed the potential of using CoNC@NC composites in environmental decontamination and antibiotic removal for wastewater treatment.

Keywords: Core-Shell ZIF-67@ZIF-90; carbonization; removing Antibiotics; ciprofloxacin; azithromycin

How to Cite: Al-Ghazzawi, F., Al-Mossawi, M. M., Al-Shawi, A., Al-Attafi, K. (2026). Synthesis and Carbonization of Core-Shell ZIF-67@ZIF-90 for Ciprofloxacin and Azithromycin Removal. *Bulletin of Chemical Reaction Engineering & Catalysis*, 21 (1), 22-37. (doi: 10.9767/bcrec.20498)

1. Introduction

The presence of pharmaceuticals in the water environment has become a serious concern for both the environment and human health [1-4]. Among them, antibiotics, such as azithromycin (AZM) and ciprofloxacin (CIP), have been frequently detected in drinking water, surface water, groundwater, and wastewater [5,6]. The extreme exposure to these antibiotics not only causes serious damage to the human body, but also can be harmful to the ecosystems and promote the dissemination of antibiotic resistance genes [7]. The incomplete removal of the antibiotics from the treated water using the traditional methods highlights an urgent need to develop efficient technologies to capture them from aqueous media. In this context, different physical and chemical methods, including membrane separation, adsorption, anaerobic reactors, chemical degradation, photocatalytic degradation, photo Fenton, electrocoagulation, and ozonation, were developed [8-10]. Among the other treatment technologies, adsorption has been considered as a promising method in the fight against water pollution owing to its high efficiency, simple operation, and cost-effectiveness [11]. Conventional adsorbents (e.g., metal oxides, zeolites, and porous carbons) often suffer from practical problems, including high cost, difficulties of regeneration, and low adsorption

* Corresponding Author.
Email: fanag83@stu.edu.iq (F. Al-Ghazzawi)

capacity [12]. Conversely, metal–organic frameworks (MOFs) composed of metal clusters and organic linkers linked by strong coordination bonds, as crystalline porous materials, offer distinct advantages [13]. Their structures can be systematically engineered and prepared to precisely control certain key adsorption-related features, including specific surface area, pore size, density, number of adsorption sites, and charge properties [14,15].

Zeolitic-imidazole frameworks (ZIFs), such as ZIF-67, ZIF-90, and ZIF-8, are a subclass of MOFs that are used efficiently in removing the organic/ inorganic pollutants from water with enhanced adsorption capacities [16]. This is due to the integration between the distinct advantages of MOFs and zeolites [17]. ZIF-67 can be considered a promising adsorbent, characterized by a high surface area, large pore size, abundant active sites, and intense attraction to guest particles [18]. Various ZIF-67-derived materials have been reported for CIP removal [19-21]. For instance, Dehghan *et al.* [21] evaluated the adsorption performance of nine MOFs, including ZIF-8, ZIF-67, and UIO-66, against CIF. Their results showed that ZIF-67-SO4 offered the highest adsorption efficiency by 99.2%.

On the other hand, ZIF-90 has an octahedral crystal structure with macropores of 11.2 Å in diameter, linked by 8 apertures with a diameter of 3.5 Å [22,23]. The high stability of ZIF-90 crystals in various circumstances makes it a promising candidate for heavy metal removal [24,25]. Zong [26] investigated the removal of heavy metals (Pb and Co) from water using a core-shell ZIF-90@chitosan/sodium alginate polysaccharide. The results showed that the maximum adsorption capacities were 1.24×10^{-3} and 1.69×10^{-3} mol/g for Pb and Co, respectively. These capacities were remarkable compared to the corresponding values reported in other studies. However, using ZIF-90 in the application of antibiotic removal has not been reported yet.

Although MOFs have notable advantages in adsorption applications, their performance is highly dependent on the number of surface free binding sites. Bimetallic MOFs have been reported to be better candidates for adsorbing antibiotics than monometallic MOFs due to their enhanced structural stability, larger surface area, and synergistic active sites [27]. Integrating two metal centers into the MOF framework not only enhances crystallinity and porosity but also increases and diversifies the adsorption sites, thereby strengthening the host–guest interaction with antibiotic molecules [28,29]. For instance, Rad *et al.* [30] prepared MIL-101-NH_2 (Fe) (monometallic MOF) and MIL-101-NH_2 (Co/Fe) (bimetallic MOF) and assessed their adsorption performance for 5-fluorouracil (5-FU) and doxorubicin (DOX). The results showed that the specific surface area of the monometallic MOF was 813 m^2/g, while the value for the optimum bimetallic MOF was 1025 m^2/g. Moreover, the maximum adsorption capacities of 5-FU and DOX by using the monometallic MOF were 485.6 and 398.3 mg/g, while these values by using the optimum bimetallic MOF were 645.4 and 538.4 mg/g. In terms of ciprofloxacin removal from water, Wei *et al.* [31] reported that using Fe/Ni-based MOFs in contaminated water can yield high ciprofloxacin adsorption capacity up to 232.1 mg/g due to the heterogeneity of the charge distribution and the existence of various binding sites induced by the bimetallic system. Luo *et al.* [32] embedded bimetallic ZnCo-ZIF in chitosan beads (ZnCo-ZIF@CS), which facilitated the efficient removal of ciprofloxacin with a high adsorption capacity of 348.9 mg/g, good recyclability, and stability in different pH and real-water samples. Liu *et al.* [33] prepared a ZIF-8/zeolite composite by the sonochemical method and investigated its removal performance of AZM under various conditions. The adsorption capacities of ZIF-8/zeolite, zeolite, and ZIF-8 were 131, 22.37, and 235.3 mg/g, respectively. The adsorption capacity of ZIF-8 was higher than that of the composite; however, the composite offered 10 regeneration cycles with removal efficiency higher than 85%, while ZIF-8 maintained such efficiency at only three regeneration cycles, indicating that the composite was more stable compared to ZIF-8.

On the other hand, the adsorption performance of MOFs is highly affected by the dimensions of their structures, with some of them exhibiting a pore size smaller than 1 nm [34]. Most antibiotics possess molecular weights in the range of 400-1200 Da [35], approximately estimated as 0.975-1.4 nm, and therefore cannot diffuse efficiently into the pore of the MOFs. Thus, adsorption predominantly takes place on the external surface of MOF particles, and a large portion of the internal surface will not be occupied by such large molecules. This would significantly reduce the accessible surface area and thereby limit the adsorption capacity of MOFs for the antibiotics, posing an extra restriction on utilizing MOFs in practical applications. To overcome this obstacle, carbonizing MOFs at high temperature and oxygen-free conditions to form porous carbon products has been proposed [36]. The carbonization process often results in raising the pore size and porosity compared to the precursors MOFs, while maintaining the same framework structure [37]. For example, the pyrolysis of ZIF-8 at 1100 °C resulted in a porous MDC-1100 with about twice the porosity of the original ZIF-8 [38]. Moreover, it was reported that derived carbon (ZnO/C 600 and ZnO/C 700) resulting from pyrolyzing MOF-5 at a high temperature retained the structure and morphology of the original MOF [39].

Various methods have been proposed to prepare carbon with a modified structure and surface chemistry to improve the adsorption ability [40]. Carbon-based composites that combine the advantages of two or more compounds can offer superior adsorption performance compared to a single material [41]. These composites can form hierarchical porous architectures that combine both micropores and mesopores, which facilitate efficient mass diffusion [41]. The hierarchical structures promote the faster diffusion of adsorbates and enhance accessibility to active sites, which can accelerate adsorption kinetics and optimize the utilization of internal and external surface areas [42]. For instance, Li *et al.* [43] prepared a C@silica core-shell composite adsorbent by carbonizing ZIF-8@silica for removing CIF from polluted water. Their findings showed that the specific surface area was 594.4 m^2/g for C@silica and 549.9 m^2/g for ZIF-8-derived carbon, while the maximum adsorption capacity was 516.8 and 430.6 mg/g for C@silica and ZIF-8-derived carbon, respectively. Therefore, it is expected that producing a unique carbon-based core-shell composite can improve the antibiotics removal performance. In addition, to the best of the author's knowledge, Carbonized MOF@MOF core@shell particles have not been investigated for the application of antibiotic removal.

From the above, it can be explored that both ZIF-67 and ZIF-90 yielded great potential in removing various organic pollutants from water. However, the adsorption performance of ZIF-67/ZIF-90 composite has not been reported yet. In this study, the distinct benefits of integrating ZIF-67 and ZIF-90 in the form of a core@shell composite were revealed by using the composite as an adsorbent for antibiotic removal applications. The novelty of this study was extended to examine the effect of the carbonization process on the performance of the proposed adsorbent. The ZIF-67@ ZIF-90 composite was first synthesized and then carbonized to produce CoNC@NC core@shell composite. Both the composites were characterized using various techniques and measurements. The adsorption performance of the two composites for CIP and AZM was investigated thoroughly. The adsorption mechanism was explored through experiments on adsorption kinetics and isotherms, which were fitted based on well-known analytical models. The effects of pH and regeneration times on the adsorption capacity of the two prepared adsorbents were also examined.

2. Materials and Methods

2.1 Materials

All materials were purchased from Sigma Aldrich Chemical, without modification: Cobalt(II) nitrate hexahydrate, $Co(NO_3)_2.6H_2O$; Zinc nitrate hexahydrate ($Zn(NO_3)_2.6H_2O$); 2-methylimidazole; imidazole-2-carboxaldehyde; methanol; N,N-dimethylformamide (DMF). The chemical pharmaceuticals, including AZM and CIP, were bought from the pharmacy.

2.2. Synthesis of ZIF-67

Crystals of ZIF-67 were synthesized by dissolving $Co(NO_3)_2.6H_2O$ (0.464 g, 1.6 mmol) in 10 mL of methanol. Then, 0.328 g (4 mmol) of 2-methylimidazole was dissolved in 10 mL of methanol. Two solutions were mixed at room temperature for 24 h. The resulting purple precipitates were collected by centrifugation and washed three times with MeOH. Finally, it was dried by vacuum at 100 ℃ [44].

2.3. Synthesis of ZIF-67@ZIF-90

For preparing ZIF-67@ZIF-90, the seed of ZIF-67 (50 mg) was dispersed in 10 mL of MeOH:H_2O (1:1) (solution A). $Zn(NO_3)_2.6H_2O$ (0.464 g, 1.6 mmol) was dissolved in 10 mL of MeOH:H_2O (1:1), and (0.328 g, 4 mmol) of imidazole-2-carboxaldehyde was dissolved in 10 mL of MeOH:H_2O (1:1). The solutions were added to a solution of ZIF-67 (solution A). The resulting solution was sonicated for 2 h, the mixture was mixed and kept in the oven for 24 h at 60℃. The core-shell ZIF-67@ZIF-90 crystals were obtained. The result was washed with MeOH three times. Finally, it was dried under vacuum at 60 ℃ [45-47].

2.4. Carbonization of ZIF-67@ZIF-90

For an optimal porous structure with large pore volume, the carbonization of the composite was conducted. The ZIF-67@ZIF-90 particles were dried overnight at 100 °C, then the particles were carbonized at 900 °C with a heating rate of 5 $°C.min^{-1}$ under argon gas for 5 hours. The temperature rose from 25 °C to reach the target temperature at 900 °C [48,49]. The product (CoNC@NC) particles were collected and used directly in adsorption experiments without washing by acid or any other activation to make a simple and environmentally friendly preparation method [48,50]. All the details of the synthesis and carbonization of ZIF-67@ZIF-90 are schematically shown in Figure 1.

2.5. Characterizations

All samples were activated under vacuum at 150 °C to remove all the solvent from the pores before characterization or use in an application. The phases of particles for all samples are determined by an X-ray diffractometer (XRD). The morphology of ZIF-67@ZIF-90 and the carbonized ZIF-67@ZIF-90 (CoNC@NC) particles were

measured by using scanning electron microscopy (SEM) and transmission electron microscopy (TEM). Raman Spectroscopy and Fourier transform infrared spectroscopy (FTIR) were used to reveal more information about the structure and surface functional groups of the carbonized samples. The thermal property of the samples was analyzed by simultaneous thermogravimetric (TGA) at 1000 °C with a heating rate of 5 °C.min^{-1}. The N_2 adsorption-desorption test was carried out at 77 °C to calculate the Brunauer–Emmett–Teller (BET) specific surface area.

2.6. Adsorption Experiments

Batch adsorption experiments were conducted to examine the adsorption performance of the proposed adsorbents for CIP and AZM from polluted water. Stock solutions of 400 mg/L CIP and 240 mg/L were prepared and then diluted to the desired initial concentration (Ci in mg/L). A 4 mg of the adsorbent was added to the CIP solution, and 20 mg of the adsorbent was added to the AZM solution to prepare the mixtures for the experiments. All the experiments were performed under a temperature of 25 ℃ and mechanical shaking at a constant speed of 180 rpm. The solution concentration of each sample was obtained by measuring the solution absorbance using UV-Vis spectrophotometer. The measurement was carried out for a small amount of the solution after the mixture was filtered through a 0.2 µm membrane. The pH of the polluted solution was adjusted using a dropwise addition of 0.01–0.1 M NaOH or HCl. To ensure the reproducibility, reliability, and statistical validity of the results, each experiment was performed in three parallel replicates.

For the adsorption kinetics experiments, the stock solutions were diluted to 50 mg/L of CIP solution and 20 mg/L of AZM solution. Certain amounts of the adsorbents were added, as previously mentioned, to the polluted solutions and samples of the mixtures, 3 mL for each, were collected and filtered to be used in the UV-Vis measurements and thus determining the concentration of the solutions at contact time t (Ct in mg/L). The samples were taken at predetermined time intervals, including 30-420 min for CIP solutions and 20-300 min for AZM

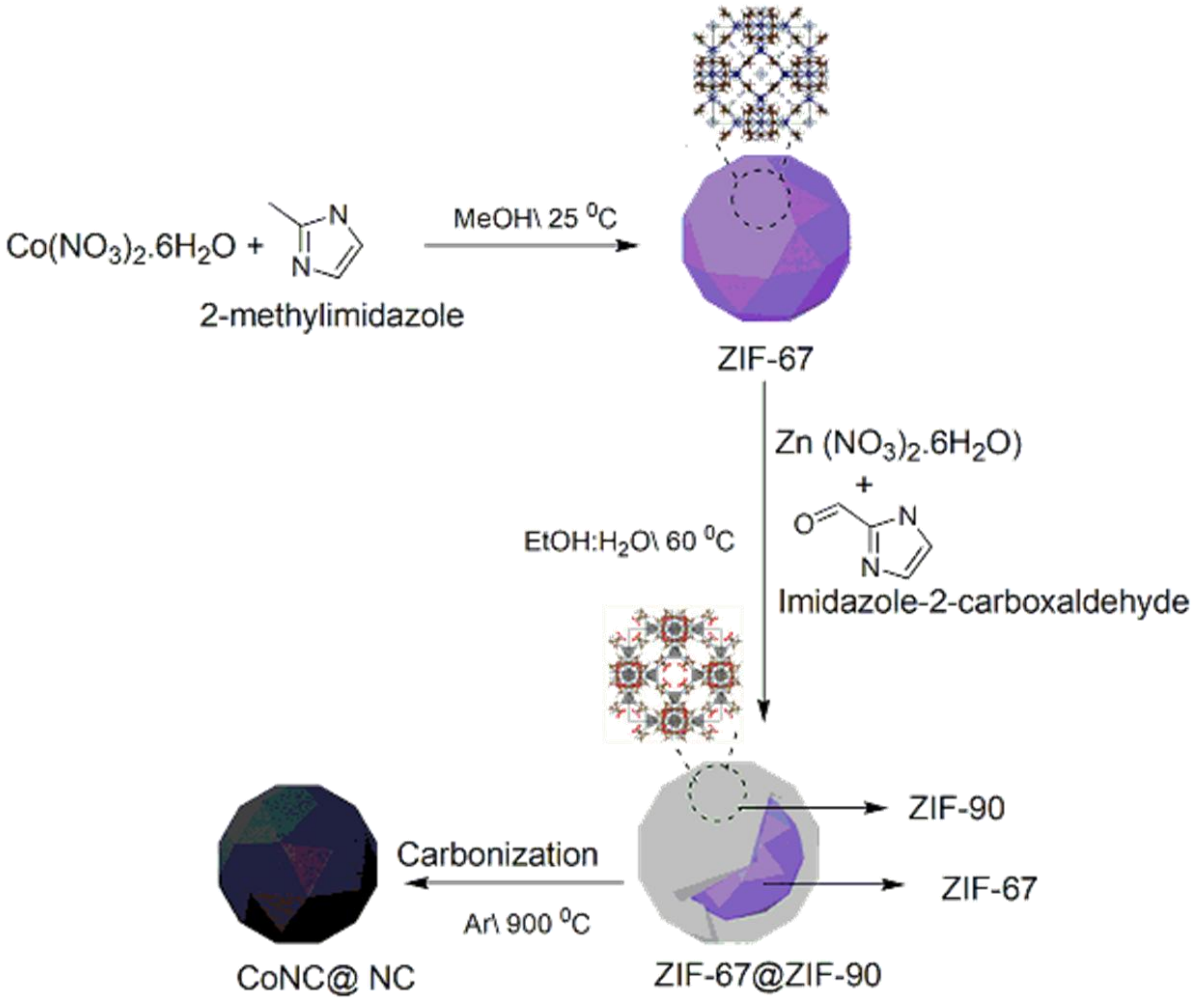

Figure 1. The schematic of the synthesis and carbonization of ZIF-67@ZIF-90 under an argon gas at 900 °C.

solutions. The pH of the solutions was maintained at 6 for the CIP solution and 7 for the AZM solution. The adsorption capacity at contact time t (Q_t in mg/g) was calculated from Equation (1) [51].

$$Q_t = \frac{(C_i - C_t) \times V}{m} \quad (1)$$

where V (L) is the volume of CIP or AZM solutions, and m (g) is the mass of the adsorbent

For the adsorption isotherms experiments, the stock solutions were diluted to various initial concentrations of CIP solution (10-260 mg/L) at a pH of 6, and of AZM solution (10-140 mg/L) at a pH of 7. Each experiment was conducted for 24 h to reach the equilibrium conditions. The equilibrium concentrations of CIP and AZM solutions (C_e in mg/L) were estimated from UV-Vis measurements when the solutions were at the equilibrium conditions. The equilibrium adsorption capacities (Q_e in mg/g) were calculated from Equation (2) [51].

$$Q_e = \frac{(C_i - C_e) \times V}{m} \quad (2)$$

For the pH effect on the adsorption performance, the equilibrium concentrations and adsorption capacities for CIP and AZM solutions were estimated under a range of pH (4-10). The other conditions of the experiments were similar to those of the adsorption kinetics experiments.

For the regeneration experiments of the adsorbents, the experiments of the adsorption isotherm were conducted under conditions similar to those of the adsorption kinetics. The solutions of CIP and AZM were filtered after reaching the equilibrium to collect the adsorbent particles. The particles were soaked in a solution of water/ethanol (20:80) for 5 h at a temperature of 25 ℃ and magnetic stirring for desorbing CIP and AZM. Afterward, the solution was filtered and the particles washed three times using ethanol and dried under vacuum at 60 ℃ for 12 h. The adsorbents were regenerated 4 times, and the adsorption test was repeated each time.

3. Results and Discussion

3.1. Characterizations

The PXRD analysis was used to study the crystallographic phase of core-shell ZIF-67@ZIF-90 crystals (Figure 2a). The patterns of ZF-67@ZIF-90 appeared diffraction peaks at 7.3°, 10.2°, 12.8°, 16.5°, and 17.6°, which agreed well

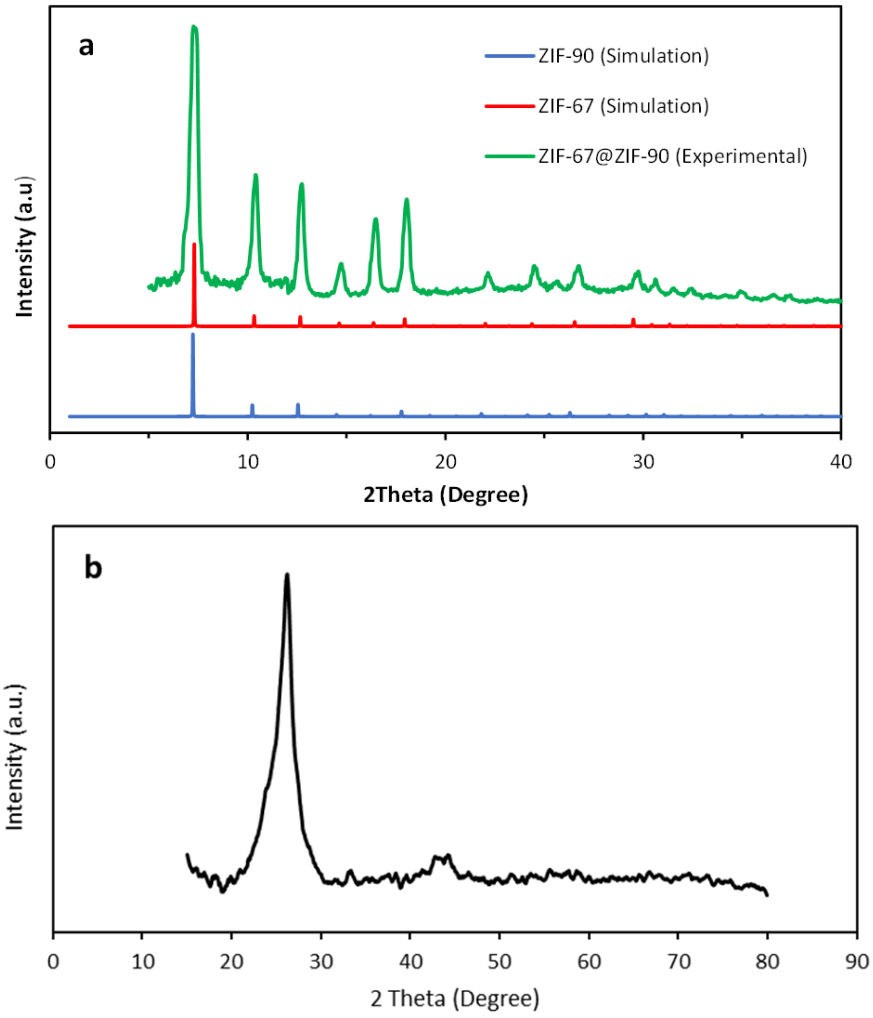

Figure 2. PXRD of (a) ZIF-67, ZIF-90 and ZIF-67@ZIF-90 and (b) CoNC@NC.

with the patterns reported in previous studies [44,45]. Furthermore, the pattern of ZIF-67@ZIF-90 exhibited behaviour similar to that of ZIF-67 and ZIF-90. This indicated the successful synthesis of the core-shell composite. However, the PXRD of CoNC@NC (Figure 2b) shows a decrease in the crystallization peaks after carbonization due to the conversion of the metal-organic frameworks to metal-carbon frameworks. It appeared as a wide-diffraction peak at 26°, which was attributed to the formation of nanoporous carbon sheets. The pattern also showed a small diffraction peak of cobalt at 43°, which may be due to the reduction of cobalt ions in the carbonized composite [52]. This pattern suggested that the diffraction peaks of the original crystals decreased dramatically after carbonization due to the increase in temperature [53]. It is worth mentioning that the XRD curve of CoNC@NC was refined using OriginLab software, and the d-spacing for the crystals was calculated at each peak as 3.345, 2.083, and 2.041 Å using Bragg's equation.

The samples of ZIF-67@ZIF-90 and CoNC@NC were analysed by SEM and TEM to identify the morphology of the crystals and determine whether any changes occurred after the carbonization process (Figure 3). In Figure 3a, the crystals of ZIF-67@ZIF-90 were in the shape of a rhombic dodecahedral, which was similar to the structure reported in previous studies [44-46]. Figure 3 (b) shows the sample after carbonization, where crystals with an approximate particle size of 1486 nm were observed, which was smaller compared to the size of the particle before carbonization (≈ 3320 nm). However, the CoNC@NC crystals sustained the same structure as the original crystals [54]. This can be attributed to the presence of ZIF-67, which can protect the topology and structure of crystals after heating at high temperature [54]. A TEM image presented in Figure 3c showed an important sign of the carbonization process as small dark coloured spots observed on the crystals, which indicated the formation of metal oxide embedded into the carbon matrix [49,54]. Overall, the crystals of ZIF-67@ZIF-90 after carbonization and forming CoNC@NC maintained the same shape of the framework. The ZIF-90 (i.e. shell) served as a cover and protector of the core and held the high temperature during the carbonization process.

The EDX analysis was conducted to reveal the different elements in the composition of ZIF-67@ZIF-90 and CoNC@NC (Figure 4). The results showed the presence of C, N, O, Co, and Zn in the ZIF-67@ZIF-90. The same elements were detected in CoNC@NC, excluding Zn, which almost

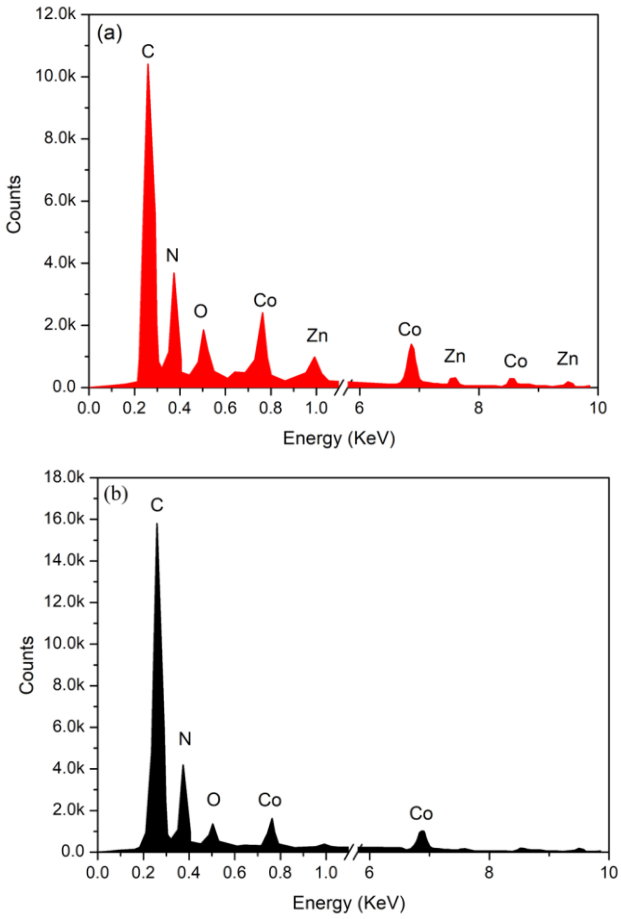

Figure 4. EDX analysis of (a) ZIF-67@ZIF-90 and (b) CONC@NC.

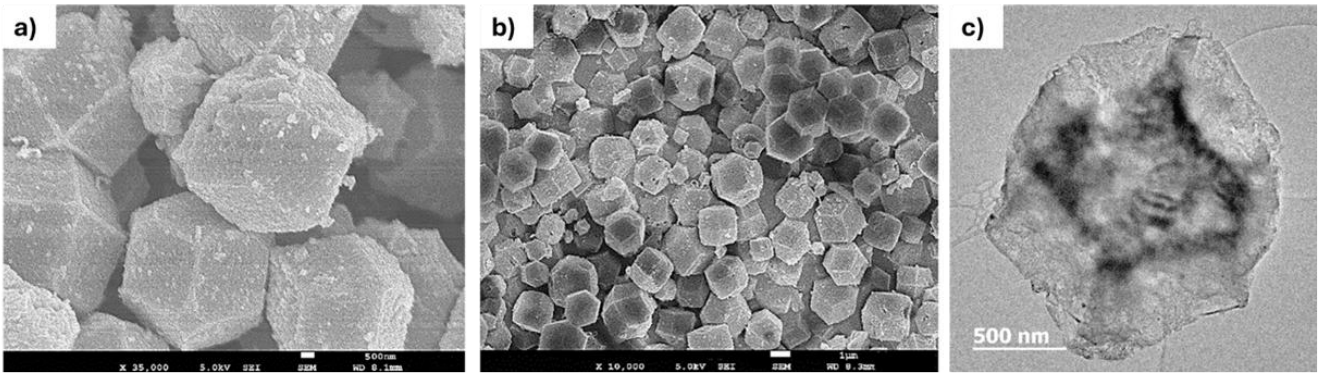

Figure 3. Illustration of (a) SEM image of core-shell ZIF-67@ZIF-90, (b) SEM image of CoNC@NC, and (c) TEM crystal image of CoNC@NC.

disappeared due to the formation of ZnO during the carbonization process [48]. In addition, as the temperature increased to 900 °C, which is very close to the boiling point of Zn (908 °C), Zn evaporated and was carried away by the argon flow [36,55].

The FT-IR spectrum of ZIF-67@ZIF-90 presented in Figure 5 shows there were stretching vibrations of C–H of aliphatic and ring imidazole at 3120 cm^{-1} and 2910 cm^{-1}, respectively, and the vibrations of C=N for imidazole of ZIF-67 were recorded at 1582 cm^{-1} [44]. There is peaks of C=O of the aldehyde group for ZIF-90 at 1670 cm^{-1} [56]. Moreover, C–N stretching of imidazole in ZIF appeared at 1340 cm^{-1} [45]. On the other hand, the spectrum of the sample after carbonization showed broad peaks related to C–N and C–O, and mostly all vibration peaks of the imidazole ligand had disappeared. That was indicative of a successful carbonization process [48].

To investigate the internal structure of CoNC@NC in detail, a Raman spectrum was obtained, and the results are presented in Figure 6. The spectrum showed two bands, including D at 1320 cm^{-1} and G at 1540 cm^{-1}. The disorder in the carbon framework was indicated by a defect bond (D-bond), and the graphitic bond (G) stated the structure of the porous carbon matrix. The intensity ratio of D peak to G peak (ID/IG) = 1.14, indicating a degree of disorder in the carbon framework with a partially ordered graphite structure. This carbon matrix is typical for carbonized MOFs and is favourable for desorption applications [57-60].

The thermogravimetric analysis (TGA) curve displayed the thermal stability of the framework for the samples (Figure 7). The TGA curve of ZIF-67@ZIF-90 showed that the first loss of weight started at a low temperature, approximately 40 °C to 150 °C, indicating the removal of solvent from the pores. After that, the TGA curve showed that the main loss of weight started at 280 °C to 300 °C, which was attributed to the decomposition of the aldehyde group in the imidazole ligand[61]. The last stage began with increasing the temperature up to 600 °C, the skeleton of the structure collapsed, and the ligand vanished [33]. Furthermore, the TGA curve of the carbonized sample (CoNC@NC) started to lose mass at lower temperatures because the samples were pre-treated at temperatures higher than 800 °C [48].

Figure 8 shows N_2 gas adsorption-desorption of the original and carbonized samples. The ZIF-67@ZIF-90 exhibited a pattern implying both type I and type IV isotherms with H1 hysteresis, indicating the presence of both micropores and mesopores in the structure [45]. This atypical hysteresis may be related to the group of

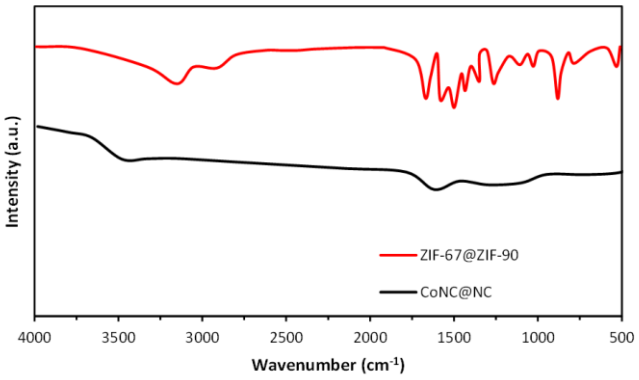

Figure 5. FT-IR spectrums of ZIF-67@ZIF-90 and CoNC@NC.

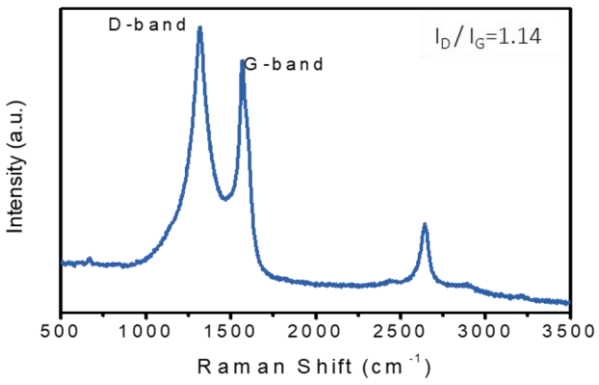

Figure 6. Raman shifting pattern of CoNC@NC.

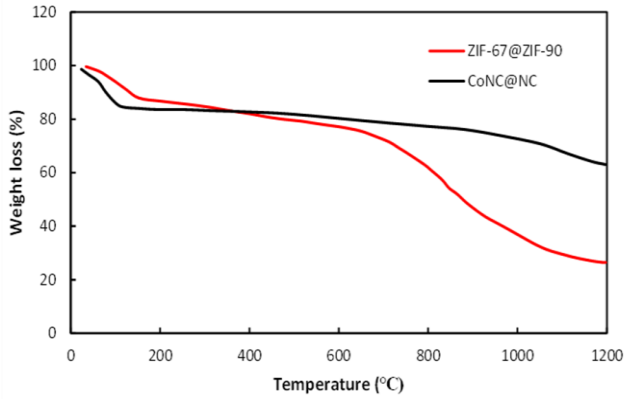

Figure 7. TGA curves of ZIF-67@ZIF-90 and CoNC@NC.

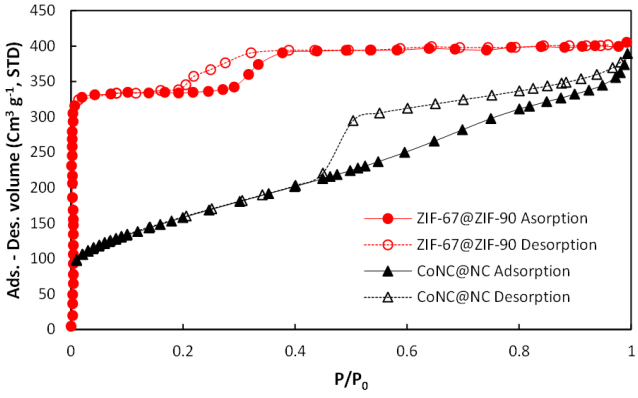

Figure 8. N_2 adsorption-desorption of ZIF-67@ZIF-90 and CoNC@NC.

aldehydes in imidazole that have free uncoordinated sites in the internal structure of ZIF-67@ZIF-90 [62]. The specific surface area of ZIF-67@ZIF-90 was 1007.812 m²/g and the pore volume was 0.627 cm³/g. For CoNC@NC, at a temperature of 900 °C, the Zinc metal in the structure of the core-shell started to vanish which led to form more mesopores and increase the porosity of the framework, Thereby the N_2 gas adsorption-desorption of the carbonized sample almost showed only type IV isotherm with H3 hysteresis which is a common feature of the mesoporous materials produced by ZIF carbonization [43]. The specific surface area of the carbonized sample decreased to 575.456 m²/g, which may be attributed to the shrinkage in the structure as evidenced by Figure 3. Table 1 summarizes the specific surface area, total volume, micro volume, and meso volume for both ZIF-67@ZIF-90 and CoNC@NC.

3.2. Adsorption Performance

3.2.1 Adsorption kinetics

The adsorption kinetics test was conducted to evaluate the impact of contact time on the adsorption capacity at various contact times (Q_t, mg/g) for ZIF-67@ZIF-90 and CoNC@NC, and to determine the equilibrium time (Figure 8). It can be seen that for all the experiments, the removal amount varied with the time until reaching the equilibrium condition. The adsorption equilibrium of ZIF-67@ZIF-90 and CoNC@NC for AZM was gradually reached within 180 min (Figure 9a), while the adsorption of CIP took longer (300 min) to reach equilibrium for both adsorbents (Figure 9b). For AZM experiments, Q_t of CoNC@NC (162.8 mg/g) was higher than that of ZIF-67@ZIF-90 (124.2 mg/g). Whereas, Q_t of CIP was 315.9 mg/g for CoNC@NC and 246.1 mg/g for ZIF-67@ZIF-90. This is due to that the carbonized adsorbent had more mesopores and active sites than those of the pristine adsorbent.

To better understand the adsorption process of ZIF-67@ZIF-90 and CoNC@NC for AZM and CIP, the pseudo-first-order (PFO) and pseudo-second-order (PSO) kinetics models were implemented to predict the curve fitting of the experimental data. The adjusted R-Square value ($R2_{adj.}$) and the equilibrium adsorption capacity (Q_e, mg/g) were used to evaluate the agreement between the predicted and observed data. Besides the fitted curves of the kinetics models presented in Figure 9, Table 2 summarizes the kinetics parameters with $R^2_{adj.}$ values of the four investigated cases. For AZM experiments, the PFO model exhibited better agreement with the observed data compared to the PSO model, indicating that the adsorption mechanism of AZM for both adsorbents was more in line with the PFO kinetics model. In contrast, for the CIP curves of both the adsorbents, the PSO model offered slightly higher $R^2_{adj.}$ values compared to the PFO model; however, the values of Q_e for PFO were much closer to the experimental values, indicating that the PFO model was more appropriate to describe the adsorption mechanism of CIP for both adsorbents. The above findings suggest that all the adsorption processes involved physisorption [63], and the adsorption mechanisms depend on the diffusion of AZM and CIP particles on the surface of ZIF-67@ZIF-90 and CoNC@NC.

3.2.2. Adsorption isotherms

The adsorption isotherms experiments were conducted to study the relationships between the equilibrium concentration (C_e) and the equilibrium adsorption capacity (Q_e) of AZM and

Table 1. The pore characteristics of ZIF-67@ZIF-90 and CoNC@NC.

Composite	S_{BET} (m²/g)	V_{total} (cm³/g)	t-plot V_{micro} (cm³/g)	V_{meso} (cm³/g)
ZIF-67@ZIF-90	1007.812	0.627	0.485	0.142
CoNC@NC	575.456	0.602	0.008	0.594

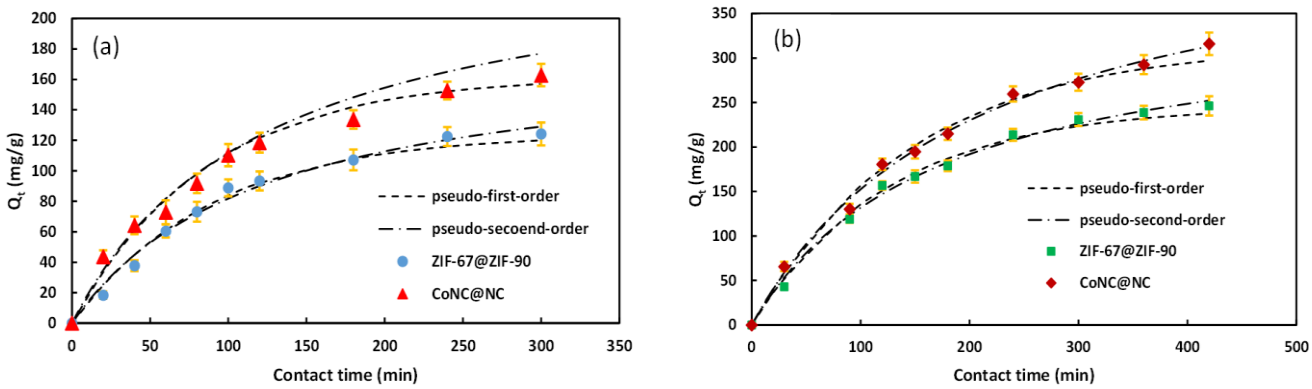

Figure 9. Adsorption kinetics of ZIF-67@ZIF-90 and C0NC@NC for: (a) AZM; (b) CIP.

CIP on ZIF-67@ZIF-90 and CoNC@NC (Figure 10). The experiments were carried out over a range of the initial concentration (C_i) of AZM and CIP. It can be observed that for all the tested cases, both Q_e and C_e increased with the increase of C_i as more adsorbate particles were offered to be extracted by the adsorbent. In addition, all the adsorption capacities of CoNC@NC for AZM and CIP were higher than the corresponding values of ZIF-67@ZIF-90. This can be attributed to the mesoporous nature of CoNC@NC. The maximum adsorption capacities (Q_m) of CoNC@NC for AZM and CIP were 255.25 and 511.2 mg/g, respectively. Whereas Q_m values of ZIF-67@ZIF-90 for AZM and CIP were 164.8 and 353.8 mg/g, respectively.

To further investigate the adsorption isotherms, two well-known isotherm models, including the Langmuir and the Freundlich models, were used to fit the experimental data of the tested cases. The fitted curves are presented in Figure 10, and the parameters of the isotherm models are summarized in Table 3. The data confirmed that AZM and CIP adsorptions were well adopted to the Langmuir model as they achieved higher values of ($R^2_{adj.}$) compared to the Freundlich model. The calculated Q_m of ZIF-67@ZIF-90 for AZM and CIP was 166.8 and 358.7 mg/g. Whereas, those values of CoNC@NC for AZM and CIP were 256.49 and 514.26 mg/g, respectively. The Langmuir isotherm model featured with formation of a single layer of adsorbates (AZM and CIP) on the homogenous surfaces of the adsorbents (ZIF-67@ZIF-90 and CoNC@NC) [64]. The particles of AZM and CIP were deduced to be extracted onto the surface of adsorbents through their active binding sites and each site could be saturated with only one particle. Therefore, the adsorption of AZM and CIP will be dominated by the availability of active sites on the surface of the adsorbents.

3.2.3. The effect of solution pH

The adsorption capacity of the adsorbent is highly dependent on the initial pH of the solution [65]. This is due to the effect of pH on the surface charges of the adsorbent and adsorbate thereby influencing the interaction between them [66]. To verify that, the effect of pH on the surface charges of ZIF-67@ZIF-90 and CoNC@NC was investigated (Figure 11), as well as the variation

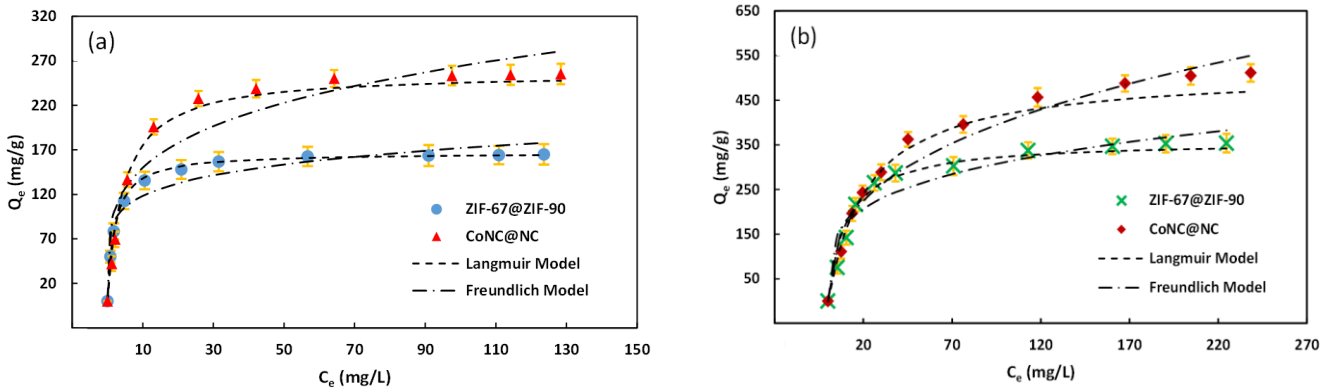

Figure 10. Adsorption isotherms of ZIF-67@ZIF-90 and CoNC@NC for: (a) AZM; (b) CIP.

Table 2. Parameters of kinetics models for different adsorbents and adsorbates.

Adsorbate	Kinetics model	Parameters	ZIF-67@ZIF-90	CoNC@NC
AZM	PFO	$Q_{e,\ Exp.}$ (mg/g)	124.2	162.8
		$Q_{e,\ Cal.}$ (mg/g)	124.43	162.16
		$K_1 \times 10^{-3}$ (min^{-1})	11.197	11.6
		$R^2_{adj.}$	0.9845	0.9853
	PSO	$Q_{e,\ Cal.}$ (mg/g)	181.47	214.88
		K_2 10^{-5} (g/mg.min)	4.53	4.63
		R^2_{adj}	0.9816	0.9764
CIP	PFO	$Q_{e,\ Exp.}$ (mg/g)	246.1	315.9
		$Q_{e,\ Cal.}$ (mg/g)	246.61	315.21
		$K_1 \times 10^{-3}$ (min^{-1})	7.898	6.807
		$R^2_{adj.}$	0.9932	0.9915
	PSO	$Q_{e,\ Cal.}$ (mg/g)	352.57	466.51
		K_2 10^{-5} (g/mg.min)	1.69	1.04
		$R_2^{adj.}$	0.9940	0.9954

of Q_e over a range of pH (4-10) was studied (Figure 12). It can be seen that the isoelectric points of ZIF-67@ZIF-90 and CoNC@NC were approximately 7.4 and 7.1, respectively. The surface charge of ZIF-67@ZIF-90 and CoNC@NC was positive under pH ranges of 4-7.4 and 4-7.1, respectively. While the surfaces were negatively charged at the ranges of 7.4-10 for ZIF-67@ZIF-90 and 7.1-10 for CoNC@NC.

On the other hand, AZM exists as cations at pH lower than 3.5, as neutral in pH range of 3.5-7.7, and as anions at pH higher than 7.7 [67]. Whereas CIP exists as cations at pH<6, as neutral in pH range of 6-9, and as anions at pH>9 [43]. For both the pristine and carbonized adsorbents, the adsorption capacity of AZM increased with the increase in pH from 4 to 7 (i.e. optimum value) as AZM maintained neutral charge and the adsorbent approached the neutral line where the highest adsorption capacity was reached. At pH>8, the adsorption capacity decreased due to the repulsion force as the charges of both the materials were negative. Moreover, the adsorption amount for CIP increased continuously as pH increased from 4 to 6, and then decreased when pH was higher than 6. The optimum adsorption amount for CIP occurred at pH of 6, which can be attributed to the charge of CIP that became neutral at pH of 6, while the charges of the adsorbents were positive. These findings suggest that the adsorption of AZM and CIP was strongly related to the charge of the adsorbent molecules.

3.2.4. Regeneration of the adsorbents

The regeneration ability of the adsorbent was studied as it is an essential property for evaluating the reusability of the adsorbent. The loaded adsorbents were regenerated using methanol and then the adsorption experiments were repeated for five cycles under the same conditions. Figure 13 shows that, for all tested cases, the adsorption capacity did not change significantly after five adsorption-desorption cycles. For instance, after 5 regeneration cycles the adsorption capacity of CoNC@NC for CIP decreased from 315.9 to 292.6 mg/g. The performance of ZIF-67@ZIF-90 for AZM and CIP was reduced by 9.2% and 8.7%. While, the reduction ratio in the performance of CoNC@NC for AZM and CIP was 9.3% and 7.4%. The results showed that the adsorbents offered a good

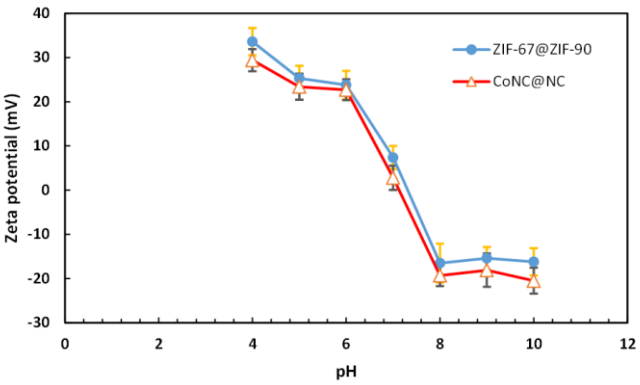

Figure 11. Variations of Zeta potential of ZIF-67@ZIF-90 and CoNC@NC with the pH.

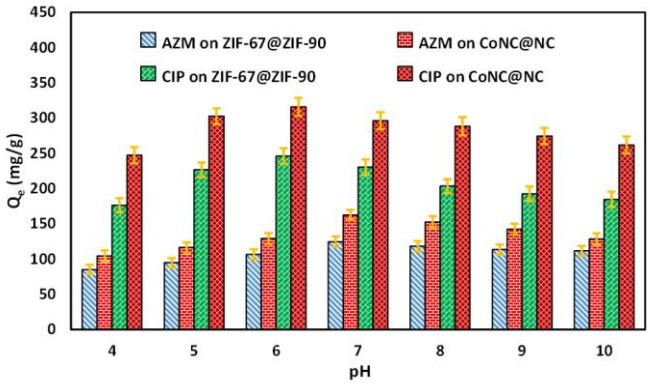

Figure 12. The adsorption capacities of ZIF-67@ZIF-90 for AZM and CIP under various pH conditions.

Table 3. Parameters of isotherm models for different adsorbents and adsorbates.

Adsorbate	Isotherm model	Parameters	ZIF-67@ZIF-90	CoNC@NC
AZM	Langmuir	$Q_{m,\,Cal.}$ (mg/g)	166.80	256.49
		K_L (L/mg)	0.4779	0.2177
		$R^2_{adj.}$	0.9982	0.9912
	Freundlich	K_F [(L/mg)$^{1/n}$.mg/g]	81.457	85.356
		n	6.1612	4.0790
		$R^2_{adj.}$	0.9348	0.9135
CIP	Langmuir	$Q_{m,\,Cal.}$ (mg/g)	358.70	514.26
		K_L (L/mg)	0.0926	0.0439
		$R^2_{adj.}$	0.9745	0.9792
	Freundlich	K_F [(L/mg)$^{1/n}$.mg/g]	96.873	76.546
		n	3.9427	2.7753
		$R^2_{adj.}$	0.9178	0.9638

regeneration performance in the adsorption of AZM and CIP from aqueous solution, reflecting an excellent potential of using them in large-scale practical applications.

3.2.5. Adsorption mechanisms

The adsorption of antibiotic particles by the adsorbents is due to the interaction between the two materials, which can be influenced by both the physical and chemical properties of the interacting materials [68]. Various mechanisms, including electrostatic interaction (EI), hydrophobic interaction (HI), hydrogen bond (HB), coordinate bond (CB), π-π interaction, and simple pore-filling, can contribute to the adsorption of antibiotics by MOF particles [69]. The adsorption possibilities of CIP and AZM by the investigated adsorbents are as follows:

(1). The difference in the surface charges of the adsorbent and the adsorbate generates EI between them, which varies based on the pH values of the solution. For instance, the highest adsorption of CIP occurred at pH of 6, which was attributed to the strong EI between CIP and the adsorbents as the CIP became neutral. In contrast, the adsorbents maintained positive charges, as evident from Figure 11.

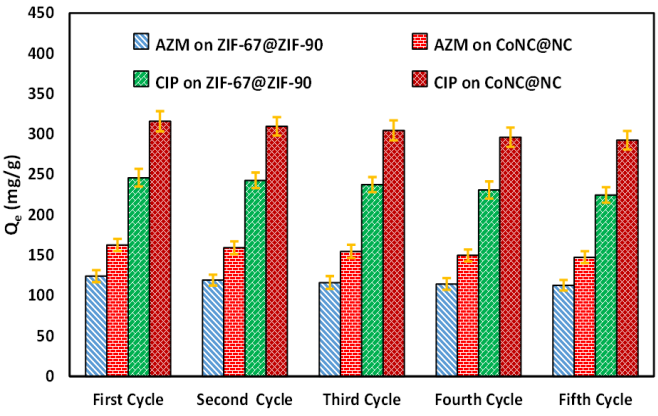

Figure 13. The regeneration performance of ZIF-67@ZIF-90 and CoNC@NC for five cycles.

(2). The hydrophobic interaction, also known as the Van der Waals interaction, is an interaction force generated between two or more hydrophobic materials. Considering the hydrophobic nature of AZM [70] and the hydrophilic nature of CIP [32], the HI contribution in the adsorption process of AZM is strong in the hydrophobic domains of the adsorbents when the value of zeta potential is close to zero. In contrast, the HI contribution of CIP is almost neglected.

(3). The functional amino and aldehyde groups in the ZIF-67@ZIF-90 tended to form hydrogen bonds with the functional groups in the antibiotics, including -NH and -COOH of CIP [71], and -OH and COOH of AZM [72].

(4). The metal ions (Co and Zn) in the adsorbents tended to form coordination metal-organic complexation with the amino or hydroxyl groups of the CIP and AZM, which have strong coordination ability for metals [73].

(5). The aromatic rings in CIP are stacked with the adsorbents through π-π interaction [32].

(6). From the adsorption kinetics and isotherms in Section 3-2, the adsorption process for both the antibiotics involved a physisorption mechanism and depended on the diffusion of the antibiotic's particles onto the surface of the adsorbents. The availability of the active binding sites on the surface of the adsorbents governs the process. To highlight the benefits of the investigated absorbents in this study, their adsorption capacity and surface area were compared to those of other MOF-based absorbents reported in the literature, as listed in Table 4.

4. Conclusions

In this study, CoNC@NC core-shell composite was successfully prepared by carbonizing ZIF-67@ZIF-90. The carbonization process was performed at 900 ℃ for 5 h under an Argon flow with a heating rate of 5 ℃/min. The original and carbonized composites were characterized using various techniques including XRD, SEM, FTIR, Raman spectroscopy, TGA and N_2 gas adsorption-

Table 4. Comparison of the adsorption capacity and surface area of the MOF-based adsorbents.

Adsorbent	Adsorbate	Max. capacity (mg/g)	Surface area (m^2/g)	Ref.
CNS@ZIF-67	CIP	40.35	203.02	[74]
$H_3PW_{12}O_{40}/Fe_3O_4$/MIL-88A (Fe)		333.33	4.16	[75]
CoFe-MOF aerogel cylinders		226.8	-	[76]
C@silica, 0.2 mL TEOS		516.8	594.4	[43]
ZIF-8 derived carbon		430.6	549.9	[43]
ZnCo-ZIF@CS		348.9	337.25	[32]
ZIF-67@ZIF90		358.7	1007.812	Current study
CoNC@NC		514.26	575.456	Current study

desorption. Both the composites were used in the batch adsorption experiments as adsorbent for removing well-known antibiotics (i.e. AZM and CIP). The carbonized composite demonstrated superior adsorption capacity and kinetics compared to the original composite. The maximum adsorption capacities of the CoNC@NC were 256.49 and 514.26 mg/g for AZM and CIP, respectively. Kinetics and isotherm adsorption results indicated that the pseudo-first-order kinetics model and Langmuir isotherm model better described the adsorption processes of both the adsorbents for AZM removal. While the adsorption behaviors of the composites toward CIP were more accurately represented by pseudo-first-order kinetics model and Langmuir isotherm model. The adsorption capacity was influenced by the pH of the solutions, and the maximum adsorption performance of the adsorbents toward AZM and CIP occurred at pH of 7 and 6, respectively. The regeneration ability of CoNC@NC was also confirmed over five experimental cycles with adsorption capacity higher than 90% of the capacity of the first cycle. This study not only demonstrates the effectiveness of these adsorbents in various environments but also offers them as a promising candidate in the applications of environmental remediation and wastewater treatment.

Acknowledgment

The first author would like to thank Southern Technical University for the administrative and technical support. During the preparation of this manuscript, the authors used Grammarly to correct grammar and spelling errors.

CRedit Author Statement

Author Contributions: F. Al-Ghazzawi: Methodology, Formal Analysis, Resources, Draft Preparation, Writing, Review and Editing, Supervision; M Al-Mossawi: Methodology, Investigation, Data Curation, Writing, Review and Editing, Visualization; A. Al-Shawi: Methodology, Investigation, Data Curation, Writing, Review and Editing; K. Al-Attafi: Methodology, Formal Analysis, Writing, Review and Editing, Supervision. The authors have read and agreed to the published version of the manuscript.

References

[1] Carabineiro, S.A.C., Thavorn-Amornsri, T., Pereira, M.F.R., Figueiredo, J.L., (2011). Adsorption of ciprofloxacin on surface-modified carbon materials. *Water Research*, 45(15), 4583-4591. DOI: 10.1016/j.watres.2011.06.008.

[2] Wada, O.Z., Olawade, D.B., (2025). Recent occurrence of pharmaceuticals in freshwater, emerging treatment technologies, and future considerations: A review. *Chemosphere*, 374, 144153. DOI: 10.1016/j.chemosphere.2025.144153.

[3] Al-Ghazzawi, F., Al-Mossawi, M.M., Allayeith, H.K., (2025). Metal–Porphyrin-Based Covalent Organic Framework Composite Membrane for Salts and Dyes Separation. *Compounds*, 5(3), 34. DOI: 10.3390/compounds5030034.

[4] Rohmatullaili, Ahmad, N., Savira, D., Erviana, D., Zultriana, Mohadi, R., Lesbani, A., (2024). A series of MgAl layer double hydroxide-based materials intercalated with Clitoria ternatea flower extract as photocatalysts in the ciprofloxacin degradation. *Chemical Physics Impact*, 8, 100587. DOI: 10.1016/j.chphi.2024.100587.

[5] Zhang, J., Xiang, S., Wu, P., Wang, D., Lu, S., Wang, S., Gong, F., Wei, X., Ye, X., Ding, P., (2022). Recent advances in performance improvement of Metal-organic Frameworks to remove antibiotics: Mechanism and evaluation. *Science of The Total Environment*, 811, 152351. DOI: 10.1016/j.scitotenv.2021.152351.

[6] Sidhu, H., O'connor, G., Mcavoy, D. (2019). Risk assessment of biosolids-borne ciprofloxacin and azithromycin. *Science of The Total Environment*, 651, 3151-3160. DOI: 10.1016/j.scitotenv.2018.10.194.

[7] Chen, X., Jiang, X., Yin, C., Zhang, B., Zhang, Q., (2019). Facile fabrication of hierarchical porous ZIF-8 for enhanced adsorption of antibiotics. *Journal of Hazardous Materials*, 367, 194-204. DOI: 10.1016/j.jhazmat.2018.12.080.

[8] Huang, A., Yan, M., Lin, J., Xu, L., Gong, H., Gong, H., (2021). A review of processes for removing antibiotics from breeding wastewater. *International Journal of Environmental Research and Public Health*, 18(9), 4909. DOI: 10.3390/ijerph18094909.

[9] Khan, P., Saha, R., Halder, G., (2024). Towards sorptive eradication of pharmaceutical micro-pollutant ciprofloxacin from aquatic environment: A comprehensive review. *Science of The Total Environment*, 919, 170723. DOI: 10.1016/j.scitotenv.2024.170723.

[10] Phoon, B.L., Ong, C.C., Saheed, M.S.M., Show, P.-L., Chang, J.-S., Ling, T.C., Lam, S.S., Juan, J.C., (2020). Conventional and emerging technologies for removal of antibiotics from wastewater. *Journal of Hazardous Materials*, 400, 122961. DOI: 10.1016/j.jhazmat.2020.122961.

[11] Crini, G., Lichtfouse, E., (2019). Advantages and disadvantages of techniques used for wastewater treatment. *Environmental Chemistry Letters*, 17(1), 145-155. DOI: 10.1007/s10311-018-0785-9.

[12] Fang, F., Lv, Q., Li, P., Tao, Y., Zhang, Y., Zhou, Y., Li, X., Li, J., (2022). Screening of hierarchical porous UiO-67 for efficient removal of glyphosate from aqueous solution. *Journal of Environmental Chemical Engineering*, 10(3), 107824. DOI: 10.1016/j.jece.2022.107824.

[13] Al-Ghazzawi, F., Conte, L., Potts, M. W., Richardson, C., and Wagner, P., (2024). Reactive Extrusion Printing of Zeolitic Imidazolate Framework Films. *ACS Applied Materials & Interfaces*, 16(33), 44270-44277. DOI: 10.1021/acsami.4c08609.

[14] Tao, Y., Fang, F., Lv, Q., Qin, W., He, X., Zhang, Y., Zhou, Y., Li, X., Li, J., (2022). Highly efficient removal of glyphosate from water by hierarchical-pore UiO-66: Selectivity and effects of natural water particles. *Journal of Environmental Management*, 316, 115301. DOI: 10.1016/j.jenvman.2022.115301.

[15] Li, J., Lv, Q., Bi, L., Fang, F., Hou, J., Di, G., Wei, J., Wu, X., Li, X., (2023). Metal-organic frameworks as superior adsorbents for pesticide removal from water: The cutting-edge in characterization, tailoring, and application potentials. *Coordination Chemistry Reviews*, 493, 215303. DOI: 10.1016/j.ccr.2023.215303.

[16] Jung, B.K., Jun, J.W., Hasan, Z., Jhung, S.H., (2015). Adsorptive removal of p-arsanilic acid from water using mesoporous zeolitic imidazolate framework-8. *Chemical Engineering Journal*, 267, 9-15. DOI: 10.1016/j.cej.2014.12.093.

[17] Saghir, S., Zhang, S., Wang, Y., Fu, E., Xiao, Z., Zahid, A.H., Pu, C., (2024). Review, recent advancements in zeolitic imidazole frameworks-67 (ZIF-67) and its derivatives for the adsorption of antibiotics. *Journal of Environmental Chemical Engineering*, 12(4), 113166. DOI: 10.1016/j.jece.2024.113166.

[18] Pattengale, B., Yang, S., Ludwig, J., Huang, Z., Zhang, X., Huang, J., (2016). Exceptionally long-lived charge separated state in zeolitic imidazolate framework: implication for photocatalytic applications. *Journal of the American Chemical Society*, 138(26), 8072-8075. DOI: 10.1021/jacs.6b04615.

[19] Liang, C., Zhang, X., Feng, P., Chai, H., Huang, Y., (2018). ZIF-67 derived hollow cobalt sulfide as superior adsorbent for effective adsorption removal of ciprofloxacin antibiotics. *Chemical Engineering Journal*, 344, 95-104. DOI: 10.1016/j.cej.2018.03.064.

[20] Alamgholiloo, H., Hashemzadeh, B., Pesyan, N. N., Sheikhmohammadi, A., Asgari, E., Yeganeh, J., Hashemzadeh, H., (2021). A facile strategy for designing core-shell nanocomposite of ZIF-67/Fe3O4: a novel insight into ciprofloxacin removal from wastewater. *Process Safety and Environmental Protection*, 147, 392-404. DOI: 10.1016/j.psep.2020.09.061.

[21] Dehghan, A., Mohammadi, A.A., Yousefi, M., Najafpoor, A.A., Shams, M., Rezania, S., (2019). Enhanced Kinetic Removal of Ciprofloxacin onto Metal-Organic Frameworks by Sonication, Process Optimization and Metal Leaching Study. *Nanomaterials*, 9(10), 1422. DOI: 10.3390/nano9101422.

[22] Huang, Z., Xiong, C., Ying, L., Wang, W., Wang, S., Ding, J., Lu, J., (2022). Facile synthesis of a MOF-derived magnetic CoAl-LDH@ chitosan composite for Pb(II) and Cr(VI) adsorption. *Chemical Engineering Journal*, 449, 137722. DOI: 10.1016/j.cej.2022.137722.

[23] Yuan, G., Tu, H., Li, M., Liu, J., Zhao, C., Liao, J., Yang, Y., Yang, J., Liu, N., (2019). Glycine derivative-functionalized metal-organic framework (MOF) materials for Co(II) removal from aqueous solution. *Applied Surface Science*, 466, 903-910. DOI: 10.1016/j.apsusc.2018.10.129

[24] Fan, C., Tang, Y., Wang, H., Huang, Y., Xu, F., Yang, Y., Huang, Y., Rong, W., Lin, Y., (2022). ZIF-90 with biomimetic Zn–N coordination structures as an effective nanozyme to mimic natural hydrolase. *Nanoscale*, 14(22), 7985-7990. DOI: 10.1039/D2NR01213H.

[25] Wei, Z., Liu, Q., Wu, C., Wang, H., Wang, H., (2018). Viscosity-driven in situ self-assembly strategy to fabricate cross-linked ZIF-90/PVA hybrid membranes for ethanol dehydration via pervaporation. *Separation and Purification Technology*, 201, 256-267. DOI: 10.1016/j.seppur.2018.03.015.

[26] Zong, P., Chen, J., Yang, Y., Qiu, Z., Xu, M., Guo, L., Lv, X., Wang, S., (2024). Outstanding performance of core–shell structured chitosan-sodium alginate decorated ZIF-90 beads for the synchronous purification of Pb and Co from industrial effluents. *Separation and Purification Technology*, 331, 125663. DOI: 10.1016/j.seppur.2023.125663.

[27] Luo, J., Luo, X., Gan, Y., Xu, X., Xu, B., Liu, Z., Ding, C., Cui, Y., Sun, C., (2023). Advantages of Bimetallic Organic Frameworks in the Adsorption, Catalysis and Detection for Water Contaminants. *Nanomaterials*, 13(15), 2194. DOI: 10.3390/nano13152194.

[28] Yang, J., Chen, Y., Cao, Y., Liu, W., Zhang, T., Zhou, H., (2024). pH-Responsive Bimetallic MOFs ZIF-8@ZIF-67 for Enhanced Antibacterial Activity. *ChemistrySelect*, 9(4), e202304908. DOI: 10.1002/slct.202304908.

[29] Kayani, K.F., (2024). Bimetallic metal–organic frameworks (BMOFs) for dye removal: a review. *RSC Advances*, 14(43), 31777-31796. DOI: 10.1039/D4RA06626J.

[30] Roshanfekr Rad, L., Faramarzi, H., Anbia, M., Irani, M., (2024). Adsorption of doxorubicin and 5-Fluorouracil anticancer drugs from aqueous media using MIL-101-NH2 (Co/Fe) bi-metal–organic framework. *Separation and Purification Technology*, 339, 126597. DOI: 10.1016/j.seppur.2024.126597.

[31] Wei, F., Wang, K., Li, W., Ren, Q., Qin, L., Yu, M., Liang, Z., Nie, M., Wang, S., (2023). Preparation of Fe/Ni-MOFs for the Adsorption of Ciprofloxacin from Wastewater. *Molecules*, 28(11), 4411. DOI: 10.3390/molecules28114411.

[32] Luo, Q., Liu, P., Bi, L., Shi, L., Zhou, J., Fang, F., Lv, Q., Fu, H., Li, X., Li, J., (2024). Selective and efficient removal of ciprofloxacin from water by bimetallic MOF beads: mechanism quantitative analysis and dynamic adsorption. *Separation and Purification Technology*, 332, 125832. DOI: 10.1016/j.seppur.2023.125832.

[33] Liu, Z., Bahadoran, A., Alizadeh, A.A., Emami, N., Al-Musaw, T.J., Alawadi, A.H.R., Aljeboree, A.M., Shamsborhan, M., Najafipour, I., Mousavi, S.E., et al., (2023). Sonocrystallization of a novel ZIF/zeolite composite adsorbent with high chemical stability for removal of the pharmaceutical pollutant azithromycin from contaminated water. *Ultrasonics Sonochemistry*, 97, 106463. DOI: 10.1016/j.ultsonch.2023.106463.

[34] Ye, Y., Xie, Y., Shi, Y., Gong, L., Phipps, J., Al-Enizi, A. M., Nafady, A., Chen, B., Ma, S., (2023). A Microporous Metal-Organic Framework with Unique Aromatic Pore Surfaces for High Performance C2H6/C2H4 Separation. *Angewandte Chemie International Edition*, 62(21), e202302564. DOI: 10.1002/anie.202302564.

[35] Bergkessel, M., Forte, B., Gilbert, I.H., (2023). Small-Molecule Antibiotic Drug Development: Need and Challenges. *ACS Infectious Diseases*, 9(11), 2062-2071. DOI: 10.1021/acsinfecdis.3c00189.

[36] Liu, B., Shioyama, H., Akita, T., Xu, Q., (2008). Metal-organic framework as a template for porous carbon synthesis. *Journal of the American Chemical Society*, 130(16), 5390-5391. DOI: 10.1021/ja7106146.

[37] Pan, J., Bai, X., Li, Y., Yang, B., Yang, P., Yu, F., Ma, J., (2022). HKUST-1 derived carbon adsorbents for tetracycline removal with excellent adsorption performance. *Environmental Research*, 205, 112425. DOI: 10.1016/j.envres.2021.112425.

[38] Ahmed, I., Bhadra, B.N., Lee, H.J., Jhung, S.H., (2018). Metal-organic framework-derived carbons: Preparation from ZIF-8 and application in the adsorptive removal of sulfamethoxazole from water. *Catalysis Today*, 301, 90-97. DOI: 10.1016/j.cattod.2017.02.011.

[39] Hu, C., Hu, X., Li, R., Xing, Y., (2020). MOF derived ZnO/C nanocomposite with enhanced adsorption capacity and photocatalytic performance under sunlight. *Journal of Hazardous Materials*, 385, 121599. DOI: 10.1016/j.jhazmat.2019.121599.

[40] Sang, X., Chen, J., Jing, M., Shi, G., Ni, C., Wang, D., Jin, W., (2019). Sustainable synthesis of nitrogen-doped porous carbon with improved electrocatalytic performance for hydrogen evolution. *New Journal of Chemistry*, 43(7), 3078-3083. DOI: 10.1039/C8NJ05819A.

[41] Li, K., Yu, L., Cai, J., Zhang, L., (2021). C@TiO2 core-shell adsorbents for efficient rhodamine B adsorption from aqueous solution. *Microporous and Mesoporous Materials*, 320, 111110. DOI: 10.1016/j.micromeso.2021.111110.

[42] Yao, Y., Zhao, X., Chang, G., Yang, X., Chen, B., (2023). Hierarchically Porous Metal–Organic Frameworks: Synthetic Strategies and Applications. *Small Structures*, 4(1), 2200187. DOI: 10.1002/sstr.202200187.

[43] Li, Y., Zeng, C., Wang, C., Zhang, L., (2018). Preparation of C@silica core/shell nanoparticles from ZIF-8 for efficient ciprofloxacin adsorption. *Chemical Engineering Journal*, 343, 645-653. DOI: 10.1016/j.cej.2018.01.147.

[44] Qian, J., Hu, C., Kong, Z., Xu, J., Wang, Y., (2022). Novel Core–Shell-Structured Zeolitic Imidazolate Framework (ZIF)-90@ ZIF-67 Applied for High-Performance All-Solid-State Asymmetric Supercapacitor. *Energy Technology*, 10(10), 2200652. DOI: 10.1002/ente.202200652.

[45] Liu, W., Zhang, Y.Q., Dong, Z.L., Chen, Z.X., Li, L., Zhao, X.Y., Wu, Y., Zhang, Y.Y., (2025). An Efficient Bifunctional Core-Shell ZIF-90@ ZIF-67 Composite as a Stable Pickering Interfacial Catalyst for the Deacetalization–Knoevenagel Tandem Reaction. *Chemistry–A European Journal*, 31(3), e202403363. DOI: 10.1002/chem.202403363.

[46] Mo, D., Wang, Z., Sun, K., Xie, X., Zhang, J., Cai, K., (2020). Core–shell metal–organic frameworks and hierarchical host–guest structures toward water-stable luminescence of lanthanide complexes in encoding beads. *Journal of Materials Chemistry C*, 8(32), 11110-11118. DOI: 10.1039/D0TC00908C.

[47] Marčec, J., Ristić, A., Logar, N.Z., (2024). New Insights into ZIF-90 Synthesis. *Molecules*, 29(16), 3731. DOI: 10.3390/molecules29163731.

[48] Abbasi, Z., Shamsaei, E., Leong, S. K., Ladewig, B., Zhang, X., Wang, H., (2016). Effect of carbonization temperature on adsorption property of ZIF-8 derived nanoporous carbon for water treatment. *Microporous and Mesoporous Materials*, 236, 28-37. DOI: 10.1016/j.micromeso.2016.08.022.

[49] Zhang, J., Yan, X., Hu, X., Feng, R., Zhou, M., (2018). Direct carbonization of Zn/Co zeolitic imidazolate frameworks for efficient adsorption of Rhodamine B. *Chemical Engineering Journal*, 347, 640-647. DOI: 10.1016/j.cej.2018.04.132.

[50] Si, Z., Cai, D., Li, S., Li, G., Wang, Z., Qin, P., (2019). A high-efficiency diffusion process in carbonized ZIF-8 incorporated mixed matrix membrane for n-butanol recovery. *Separation and Purification Technology*, 221, 286-293. DOI: 10.1016/j.seppur.2019.04.004.

[51] Xiong, G., Wang, B.-B., You, L.-X., Ren, B.-Y., He, Y.-K., Ding, F., Dragutan, I., Dragutan, V., Sun, Y.-G., (2019). Hypervalent silicon-based, anionic porous organic polymers with solid microsphere or hollow nanotube morphologies and exceptional capacity for selective adsorption of cationic dyes. *Journal of Materials Chemistry A*, 7(1), 393-404. DOI: 10.1039/C8TA07109H.

[52] Wang, R., Lou, M., Zhang, J., Sun, Z., Li, Z., Wen, P., (2021). Zif-8@ zif-67-derived co embedded into nitrogen-doped carbon nanotube hollow porous carbon supported pt as an efficient electrocatalyst for methanol oxidation. *Nanomaterials*, 11(10), 2491. DOI: 10.3390/nano11102491.

[53] Baghban, A., Ezedin Nejadian, H., Habibzadeh, S., Zokaee Ashtiani, F., (2022). Hydrogenation of pyrolysis gasoline by novel Ni-doped MOF derived catalysts from ZIF-8 and ZIF-67. *Scientific Reports*, 12(1), 19428. DOI: 10.1038/s41598-022-24071-2.

[54] Wang, Y., Wang, K., Zhang, X., Li, J., (2023). Co@ NC@ ZIF-8-hybridized carbon molecular sieve membranes for highly efficient gas separation. *Journal of Membrane Science*, 682, 121781. DOI: 10.1016/j.memsci.2023.121781.

[55] Zhang, P., Sun, F., Xiang, Z., Shen, Z., Yun, J., Cao, D., (2014). ZIF-derived in situ nitrogen-doped porous carbons as efficient metal-free electrocatalysts for oxygen reduction reaction. *Energy & Environmental Science*, 7(1), 442-450. DOI: 10.1039/C3EE42799D.

[56] Cao, Q., Kang, S., Lu, C., Sun, D., Li, J., Chen, H., Li, X., Zhang, Y., (2025). Preparation and characterization of the octadecylamine-loaded microcapsule through incorporation of ZIF-90-PDA for self-healing and anti-corrosion coatings. *Construction and Building Materials*, 489, 142171. DOI: 10.1016/j.conbuildmat.2025.142171.

[57] Liu, Q., Zhang, H., Zhang, K., Li, J., Cui, J., Shi, T., (2024). Iron–Cobalt Bimetallic Metal–Organic Framework-Derived Carbon Materials Activate PMS to Degrade Tetracycline Hydrochloride in Water. *Water*, 16(20), 2997. DOI: 10.3390/w16202997.

[58] Chen, J.-J., Chen, Y.-T., Senthil Raja, D., Kang, Y.-H., Tseng, P.-C., Lin, C.-H., (2015). Metal-organic frameworks to metal/metal oxide embedded carbon matrix: Synthesis, characterization and gas sorption properties. *Materials*, 8(8), 5336-5347. DOI: 10.3390/ma8085245.

[59] Ren, S., Ju, P., Yu, H., Nan, B., Wang, L., Lian, A., Zang, X., Liang, H., (2024). Preparation of Metal–Organic-Framework-Derived Fe-CN@ CoCN Nanocomposites and Their Microwave Absorption Performance. *Coatings*, 14(1), 133. DOI: 10.3390/coatings14010133.

[60] Wei, Z., Pan, R., Hou, Y., Yang, Y., and Liu, Y., (2015). Graphene-supported Pd catalyst for highly selective hydrogenation of resorcinol to 1, 3-cyclohexanedione through giant π-conjugate interactions. *Scientific Reports*, 5(1), 15664. DOI: 10.1038/srep15664.

[61] Yuan, H., Wu, Y., Pan, X., Gao, L., Xiao, G., (2020). Pyridyl ionic liquid functionalized ZIF-90 for catalytic conversion of CO2 into cyclic carbonates. *Catalysis Letters*, 150(12), 3561-3571. DOI: 10.1007/s10562-020-03259-z.

[62] Liu, C., Yan, B., (2015). Luminescent zinc metal—Organic framework (ZIF-90) for sensing metal ions, anions and small molecules. *Photochemical & Photobiological Sciences*, 14(9), 1644-1650. DOI: 10.1039/c5pp00107b.

[63] Rudzinski, W., Plazinski, W., (2006). Kinetics of solute adsorption at solid/solution interfaces: a theoretical development of the empirical pseudo-first and pseudo-second order kinetic rate equations, based on applying the statistical rate theory of interfacial transport. *The Journal of Physical Chemistry B*, 110(33), 16514-16525. DOI: 10.1021/jp061779n.

[64] Bolster, C.H., Hornberger, G. M., (2007). On the use of linearized Langmuir equations. *Soil Science Society of America Journal*, 71(6), 1796-1806. DOI: 10.2136/sssaj2006.0304.

[65] Feng, J.-B., Li, Y.-Y., Zhang, Y., Xu, Y.-Y., Cheng, X.-W., (2022). Adsorptive removal of indomethacin and diclofenac from water by polypyrrole doped-GO/COF-300 nanocomposites. *Chemical Engineering Journal*, 429, 132499. DOI: 10.1016/j.cej.2021.132499.

[66] Hasan, Z., Choi, E.-J., Jhung, S.H., (2013). Adsorption of naproxen and clofibric acid over a metal–organic framework MIL-101 functionalized with acidic and basic groups. *Chemical Engineering Journal*, 219, 537-544. DOI: 10.1016/j.cej.2013.01.002.

[67] Upoma, B.P., Yasmin, S., Ali Shaikh, M.A., Jahan, T., Haque, M.A., Moniruzzaman, M., Kabir, M.H., (2022). A Fast Adsorption of Azithromycin on Waste-Product-Derived Graphene Oxide Induced by H-Bonding and Electrostatic Interactions. *ACS Omega*, 7(34), 29655-29665. DOI: 10.1021/acsomega.2c01919.

[68] Hasan, Z., Khan, N.A., Jhung, S.H., (2016). Adsorptive removal of diclofenac sodium from water with Zr-based metal–organic frameworks. *Chemical Engineering Journal*, 284, 1406-1413. DOI: 10.1016/j.cej.2015.08.087.

[69] Zhao, X., Zheng, M., Gao, X., Zhang, J., Wang, E., Gao, Z., (2021). The application of MOFs-based materials for antibacterials adsorption. *Coordination Chemistry Reviews*, 440, 213970. DOI: 10.1016/j.ccr.2021.213970.

[70] Pouretedal, H.R., (2014). Preparation and characterization of azithromycin nanodrug using solvent/antisolvent method. *International Nano Letters*, 4(1), 103. DOI: 10.1007/s40089-014-0103-x.

[71] Zhao, R., Ma, T., Zhao, S., Rong, H., Tian, Y., Zhu, G., (2020). Uniform and stable immobilization of metal-organic frameworks into chitosan matrix for enhanced tetracycline removal from water. *Chemical Engineering Journal*, 382, 122893. DOI: 10.1016/j.cej.2019.122893.

[72] Patil, M., Singh, S., Kumari, D., Daverey, A., Dutta, K., (2024). Adsorption of azithromycin antibiotic from water onto biochar derived from Terminalia chebula and sugarcane bagasse. *Water Practice and Technology*, 19(8), 2973-2990. DOI: 10.2166/wpt.2024.140.

[73] Li, B., Zhang, Y., Xu, J., Fan, S., Xu, H., (2022). Facile preparation of magnetic porous biochars from tea waste for the removal of tetracycline from aqueous solutions: Effect of pyrolysis temperature. *Chemosphere*, 291, 132713. DOI: 10.1016/j.chemosphere.2021.132713.

[74] Bhattacharyya, P., Sarma, L., Taneja, A., Parmar, P.R., Jain, G., Bandyopadhyay, D., Chakrabarti, S., (2023). MOF-heterostructure-mediated pH-responsive adsorptive removal of ciprofloxacin: a step towards pharmaceutical wastewater treatment. *ChemNanoMat*, 9(4), e202200518. DOI: 10.1002/cnma.202200518.

[75] Ashrafi, M., Farhadi, S., (2023). Polyoxometalate supported on a magnetic Fe3O4/MIL-88A rod-like nanocomposite as an adsorbent for the removal of ciprofloxacin, tetracycline and cationic organic dyes from aqueous solutions. *RSC Advances*, 13(10), 6356-6367. DOI: 10.1039/d2ra07898h.

[76] Tran, T.K.N., Tran, A.C., Tran, T.T.N., Le, T.H.N., Lam, V.T., (2023). Optimization of ciprofloxacin adsorption onto CoFe-MOF aerogel cylinders based on response surface methodology: adsorption kinetics, isotherm models. *Materials Science and Engineering: B*, 297, 116694. DOI: 10.1016/j.mseb.2023.116694.